Internal kink mode stability in the presence of ICRH driven fast ions populations

F. Nabais 1), D. Borba 1), M. Mantsinen 2), M. F. F. Nave 1), S. Sharapov 3) and JET-EFDA contributors[†]

1) Association EURATOM/IST, Av. Rovisco Pais, 1049-001 Lisboa, Portugal
2) Association EURATOM/TEKES, Helsinki University of Technology, Espoo, Finland
3) EURATOM/UKAEA Fusion Association, Culham Science Centre, Abingdon, OX14 3DB, U.K.

e-mail contact of the main author: fnabais@cfn.ist.utl.pt

Abstract. The internal kink mode is commonly present in tokamak plasmas and is often responsible for sawtooth instabilities. The presence of fast ions in the plasma, such as those generated by auxiliary heating, may not only affect sawtooth behaviour but also cause the appearance of fishbone oscillations which are caused by different branches of the internal kink dispersion relation. There are principally two different methods that are used to analyse the internal kink mode stability in the presence of fast ions. The first is based on a perturbative approach and in this case, the fast ions' energy functional is taken as a perturbation of the ideal MHD functional. The use of numerical codes like the new version of the CASTOR-K code then allows an accurate calculation of the perturbation on the mode growth rate. The second method is based on a variational formulation where the full dispersion equation including diamagnetic effects is solved using simplified expressions for the fast ions' energy functional and the fast ions' distribution function. The marginal stability equation allows then the determination of the regions of stability for each of the solutions in the space of parameters. In this paper both methods are described and applied to analyse JET experiments were both sawteeth and fishbone stability changed during the discharge.

1. Introduction

Internal kink modes are commonly observed in tokamak experiments. The most unstable is the n=1, m=1 (toroidal and poloidal mode numbers) which is associated with the q=1 surface, q being the safety factor. This mode is always unstable in cylindrical geometry if the safety factor on axis q_0 is below unity and though toroidal effects are stabilizing, the mode is still potentially unstable in all tokamaks. It is often associated with the occurrence of sawteeth [1], but fishbone oscillations [2] can also be caused by different branches of the internal kink dispersion relation [3]. In future tokamaks like ITER, where the q=1 radius is expected to be large, instabilities caused by n=1, m=1 internal kink modes can involve the displacement of large portions of plasma. These instabilities may reduce the discharge's performance and, aside from that, the occurrence of a monster sawtooth crash after a period of stabilization can be hazardous. It is therefore important not only predict when the different branches of the dispersion relation can be unstable but also try and develop methods to control the related instabilities. The presence in the plasma of ICRH driven fast ions is known to strongly affect the internal kink stability [4]. These ions, under usual conditions of tokamak operation, are predicted to have a destabilizing effect over fishbones and a stabilizing effect over sawteeth. However, it is possible to change heating characteristics or plasma parameters in order to modify these effects, allowing some control over these instabilities. In the ideal MHD framework, when the minimized variational energy for the internal kink displacement [5] is negative, $\delta W_{MHD} < 0$, the normal modes problem allows two solutions, one stable and one

[†] See appendix of J. Pamela et al., "Overview of JET Results" OV/1-2, Fusion Energy 2004, IAEA, (2004)

unstable, both with $\mathrm{Re}(\omega)=0$, where ω is the complex frequency. The unstable solution will be referred to as the kink mode and its growth rate is given by $\gamma_I=-\omega_A\delta W_{MHD}$, where ω_A is the Alfven frequency. The stable solution $\mathrm{Im}(\omega)<0$, if physical, corresponds to the ion mode. γ_I is then defined as the growth rate of the unstable mode associated with $\delta W_{MHD}<0$. Taking into account diamagnetic effects, the dispersion relation for the internal kink mode is given by $\gamma_I+i[\omega(\omega-\omega_{*i})]^{1/2}=0$ [6], where ω_{*i} is the bulk ion diamagnetic frequency. If ω_{*i} is finite, the kink and ion modes are no longer purely growing (damped) and acquire real frequencies. When increasing ω_{*i} the growth and damping rates of the kink and ion branches decrease until for $\omega_{*i}>2\gamma_I$ both branches become marginally stable. If the plasma contains fast particles, these particles can provide a viscous effect that taps the energy related to the bulk ions' density gradient destabilizing the ion branch. This branch, when unstable, causes fishbone bursts to be observed with a mode frequency $\mathrm{Re}(\omega)\approx\omega_{*i}$ [7], [8]. Including the hot particles' energy functional δW_{HOT} in the dispersion relation a new branch appears in its solution, the (precessional drift) fishbone branch [9]. The growth rate of this mode goes to $-\infty$ as the fast particles β (kinetic pressure / magnetic pressure) goes to zero but becomes unstable when β_h is above a critical value $\beta_h>\beta_{hc}$. This branch is responsible for fishbone oscillations with a mode frequency $\mathrm{Re}(\omega)\approx\langle\omega_D\rangle$, where $\langle\omega_D\rangle$ is the average precessional drift of fast ions. Usually the regime of low frequency fishbones $\mathrm{Re}(\omega)\approx\omega_{*i}$ (diamagnetic fishbones will be adopted here) is observed for low values of β_h while the regime of high frequency fishbones $\mathrm{Re}(\omega)\approx\langle\omega_D\rangle$ (precessional fishbones) is observed for high values of β_h being both regimes separated by a stable window on β_h [10].

In this paper it is analysed how ICRH driven fast ion populations can affect the n=1, m=1 internal kink stability through the inclusion of the hot particles energy functional δW_{HOT} in the appropriate equations. For this two different methods are used. The first is based on a perturbative approach, δW_{HOT} being taken as a perturbation of the ideal MHD functional δW_{MHD}. The use of numerical codes then allows an accurate calculation of δW_{HOT} as a function of several parameters. In the limit $\omega/\langle\omega_D\rangle\to 0$ it is possible to evaluate how sawtooth stabilization by fast ions depends on these parameters. The second method is based on a variational formulation where the full dispersion equation is solved for a large aspect ratio circular cross-section, using simplified expressions for the fast ions' energy functional and fast ions' distribution function. The marginal stability equation allows then the determination of the regions of stability for each branch of the internal kink dispersion relation in the space of parameters.

2. Method perturbative

The effect of a fast ion population on the kink mode can be analysed using a perturbative approach where δW_{HOT} is taken as a perturbation of the ideal MHD functional δW_{MHD},

$$\delta W=\delta W_{MHD}+\delta W_{HOT}. \tag{1}$$

The eigenfunction is determined by minimizing only the MHD functional δW_{MHD} and is later used to calculate δW_{HOT}. With this it is possible to accurately calculate δW_{HOT} using numerical codes. A new version of the CASTOR-K [11] code has recently been developed in order to calculate δW_{HOT} for ICRH driven fast ion populations. The CASTOR-K code uses the eigenfunction calculated by the ideal MDH code MISHKA [12] or the resistive MHD code CASTOR [13] and the equilibrium calculated by the HELENA code [14]. The fast ion distribution function is assumed to be characterized by a single value of the normalized magnetic momentum $\lambda=\mu B_0/E$, where μ is the magnetic momentum $\mu=mv_\perp^2/2B$, B_0 is

the magnetic field on axis and E is the particle energy. This corresponds to considering a population of particles with potato orbits ($P_\phi < 0$) and banana orbits with turning points located over the ICRH resonant layer, λ being given by the ratio between the ICRH resonance radius and the major radius $\lambda = R_{res}/R$. The energy distribution is assumed to be a Maxwellian characterized by a temperature T_{HOT} and the radial distribution is introduced as a polynomial function of adjustable parameters. In the limit $\omega/\langle\omega_D\rangle \to 0$ the perturbation on the mode growth rate due to fast ions is given by:

$$\gamma_{HOT} = -\frac{1}{2\gamma_I}\frac{\mathrm{Re}\,\delta W_{HOT}}{E_k}, \tag{2}$$

where E_k is the kinetic energy of the mode. This limit is adequate to study the effect of fast ions on sawtooth stability. The new version of the CASTOR-K code calculates both the adiabatic part δW_{HOT}^{ad} and the non-adiabatic part δW_{HOT}^{na} of the fast ions' functional δW_{HOT} taking into account the large size of their banana orbits and potato orbits [15],

$$\delta W_{HOT}^{ad} = \frac{2\pi^2}{\Omega m^2}\sum_\sigma \int dE d\mu dP_\varphi (\xi\cdot\nabla\psi)\frac{Ze}{c}\frac{\partial F}{\partial P_\varphi}, \tag{3}$$

$$\delta W_{HOT}^{na} = -\frac{2\pi^2}{\Omega m^2}\sum_\sigma \int dE d\mu dP_\varphi \tau_b(\omega - n\omega_*)\frac{\partial F}{\partial E}\sum_{p=-\infty}^{\infty}\frac{|Y_p|^2}{\omega + n\langle\dot{\varphi}\rangle + p\omega_b}. \tag{4}$$

The adiabatic part of δW_{HOT} traduces a fluid effect that is expected to be destabilizing. The non-adiabatic part of δW_{HOT}, in the limit $\omega/\langle\omega_D\rangle \to 0$, is mainly due to the conservation of the third adiabatic invariant and is usually stabilizing. Sawtooth stabilization can then occur if this stabilizing effect is strong enough to overcome destabilizing effects. The CASTOR-K code allows δW_{HOT} to be calculated as function of several parameters, like the fast ions' temperature T_{HOT}, the location of the ICRH resonant layer ($\lambda = R_{res}/R$), the safety factor on axis (or the q=1 radius assuming a fixed q profile) and the fast ions' radial profile. Thus, it is possible to analyse the dependence of sawtooth stabilization by fast ions on any of these parameters. As an example, Fig. 1 shows the perturbation on the kink mode growth rate originated by the non-adiabatic part of δW_{HOT} as a function of the safety factor on axis (or q=1 radius having assumed a fixed q profile) and the fast ions' temperature T_{HOT} for a typical JET equilibrium with on-axis heating. Numerical results show that for relatively small values of the q=1 radius r_1, the stabilizing effect related with the non-adiabatic part of δW_{HOT} tends to disappear as T_{HOT} increases but when the q=1 radius is large the stabilizing effect does not vanish. In this case the size of the fast particles' orbits is still small when compared to that of the q=1 radius r_1. Numerical simulations also show that when the q=1 radius is very small, the stabilizing effect of particles with potato orbits ($P_\phi < 0$) becomes increasingly important. The adiabatic part of δW_{HOT} gives a destabilizing contribution that increases with T_{HOT}.

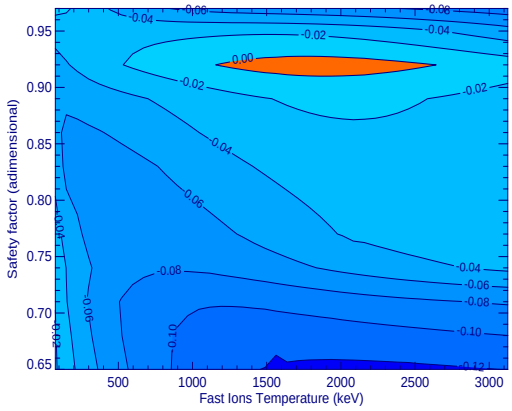

Figure 1: Perturbation on the kink mode growth rate due to the non adiabatic part δW_{HOT}^{na} as function of the fast ions temperature and safety factor on axis for a fast ions profile peaked in the center. Blue regions are stabilizing and red destabilizing.

3. Method variational

Another possible approach is to solve the full variational problem making the necessary simplifications. The dispersion relation including fast ion, resistive and finite Larmor radius effects for a large aspect ratio circular cross-section is given by [3], [16-19],

$$\delta W_{MHD} + \delta W_{HOT} - \frac{8i\Gamma\left[\left(\Lambda^{3/2}+5\right)/4\right]\left[\omega\left(\omega-\omega_{*i}\right)\right]^{1/2}}{\Lambda^{9/4}\Gamma\left[\left(\Lambda^{3/2}-1\right)/4\right]\omega_A} = 0 \qquad (5)$$

where, $\Lambda = -i\left[\omega\left(\omega-\hat{\omega}_{*e}\right)\left(\omega-\omega_{*i}\right)\right]^{1/3}/\gamma_R$, $\gamma_R = S^{-1/3}\omega_A$ is the resistive growth rate, S is the magnetic Reynolds number, ω_A is the Alfven frequency, ω_{*e} is the electron diamagnetic frequency $\omega_{*e} = \left(en_eBr\right)^{-1} dP_e/dr$, P_e and n_e are the electron pressure and density respectively and $\hat{\omega}_{*e} = \omega_{*e} + 0.71\left(eBr\right)^{-1} dT_e/dr$. The Euler gamma functions in equation (5) come from the inertial layer and are evaluated at the q=1 surface. For a Maxwellian distribution in energy and a population characterized by a single normalized magnetic momentum $\lambda = 1$ (on-axis heating), in the ideal limit the threshold condition $\mathrm{Im}(\omega) = 0$, i.e. the condition for which the stability of the mode changes, is given by

$$\gamma_I = \frac{3}{4}\left[\frac{\omega}{\langle\omega_D\rangle}\left(\frac{\omega}{\langle\omega_D\rangle}-\frac{\omega_{*i}}{\langle\omega_D\rangle}\right)\right]^{\frac{1}{2}}\left(\frac{\omega}{\langle\omega_D\rangle}\right)^{-\frac{3}{2}}\left[\frac{1}{2}+\frac{\omega}{\langle\omega_D\rangle}+\left(\frac{\omega}{\langle\omega_D\rangle}\right)^{\frac{3}{2}}\mathrm{Re}\,Z\left[\left(\frac{\omega}{\langle\omega_D\rangle}\right)^{\frac{1}{2}}\right]\right], \qquad (6)$$

with the corresponding value of β_h given by,

$$\beta_h = \frac{3}{4}\frac{\varepsilon\omega_A}{\pi^{1/2}\langle\omega_D\rangle}\left[\frac{\omega}{\langle\omega_D\rangle}\left(\frac{\omega}{\langle\omega_D\rangle}-\frac{\omega_{*i}}{\langle\omega_D\rangle}\right)\right]^{\frac{1}{2}} e^{\omega/\omega_D}\left(\frac{\omega}{\langle\omega_D\rangle}\right)^{-\frac{5}{2}}. \qquad (7)$$

When ω_{*i} and $\langle\omega_D\rangle$ are of the same order of magnitude, β_h is a monotonic function of ω and equation (6) has two solutions provided that $\gamma_I < \gamma_M$, where γ_M is the maximum possible value for the right hand side of equation (6). With this it is possible to determine the regions of stability for each branch of the internal kink dispersion relation (5) in the space of parameters ($\gamma_I, \omega_{*i}, \beta_h$). The stability diagram in the plan (γ_I, β_h), with ω_{*i} as a parameter, is presented in Fig 2.

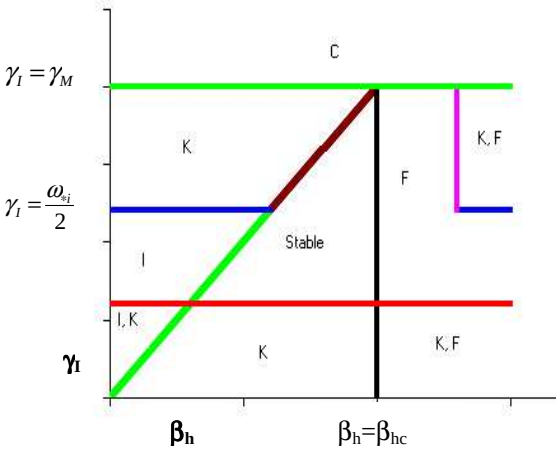

Figure 2: Regions of stability for the different branches of the internal kink dispersion relation in the space of parameters ($\beta_h, \gamma_I, \omega_{*i}$). In regions labelled with a K the kink branch is unstable, with an I the ion branch is unstable and with an F the fishbone branch is unstable. In region C the fishbone branch coalesces with one of the low frequency branches (in this case the kink branch).

To complete the diagram, the lines corresponding to sawtooth destabilization due to finite orbit width effects and resistive effects are added to the diagram, since these effects are not included

in equation (6). Resistive effects are only important when γ_I is small, making the kink branch unstable. Finite orbit width effects may reduce the efficiency of stabilization by fast ions also allowing the kink branch to be unstable. With this, it is possible to analyse qualitatively (or predict) the stability of the different branches during a discharge, if the evolution of the parameters ($\gamma_I, \omega_{*i}, \beta_h$) is known or could be estimated. The growth rate of the precessional fishbone mode can be calculated by numerical code that has been recently developed [20].

4. Applications - Sawteeth

Recent JET experiments with ICRH only and low density plasmas have shown that sawteeth were stabilized when the plasma density was increased above a threshold value [21]. Sawteeth were also stable during the initial part of the ICRH ramp phase and were destabilized as the ICRH power increased (see Fig. 3). Comparing the equilibrium conditions and the mode eigenfunction calculated by the MISHKA code no significant changes could be found between the situations where sawteeth were stable and unstable. This suggested the loss of stabilization at low plasma densities should be related with changes in the fast ions distribution function. Since the ICRH resonant layer was not moved and changes in the radial distribution were not expected, changes in sawteeth behaviour must have been related to changes in the fast ions energies. In fact, the Stix model [22] predicts the fast ions temperature to be proportional to the ratio between the volume-averaged ICRH power density and the plasma density $\langle P_{ICRH} \rangle / n_e$. Calculations of the temporal evolution of the fast ions temperature T_{HOT} have shown that sawteeth destabilization during the ICRH ramp phase coincided with an increase in T_{HOT} and the later stabilization coincided with a decrease in T_{HOT}. Numerical simulations with the CASTOR-K code have confirmed that for these specific discharges the stabilizing effect of δW_{HOT}^{na} over sawteeth decreases significantly as the fast ions temperature T_{HOT} increases, while on the other hand the destabilizing effect of δW_{HOT}^{ad} increases. It is then plausible that for sufficiently high fast ions temperatures δW_{HOT}^{na} becomes too small to overcome the destabilizing effects.

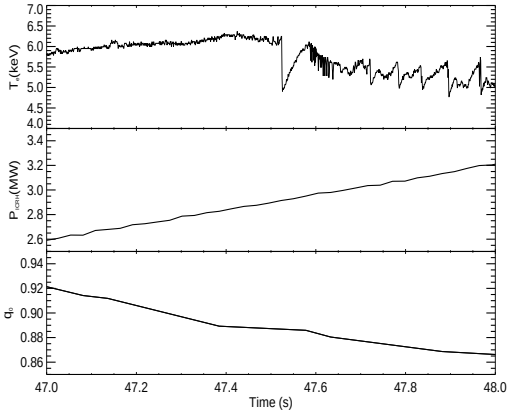

Figure 3: Temporal evolution of the electronic temperature, ICRH power and safety factor on axis during the RF ramp phase in pulse #54306.

5. Applications - Fishbones

In the same set of experiments fishbone activity was also observed along with sawteeth. Periods of frequent sawteeth crashes were always accompanied by high frequency precessional fishbones with a frequency $\mathrm{Re}(\omega) \approx \langle \omega_D \rangle$. When sawteeth were stabilized and frequent crashes ceased, these fishbone bursts were gradually replaced by low frequency diamagnetic fishbones $\mathrm{Re}(\omega) \approx \omega_{*i}$. The occurrence of a monster sawtooth crash restored the original high frequency fishbones (see Fig. 4).

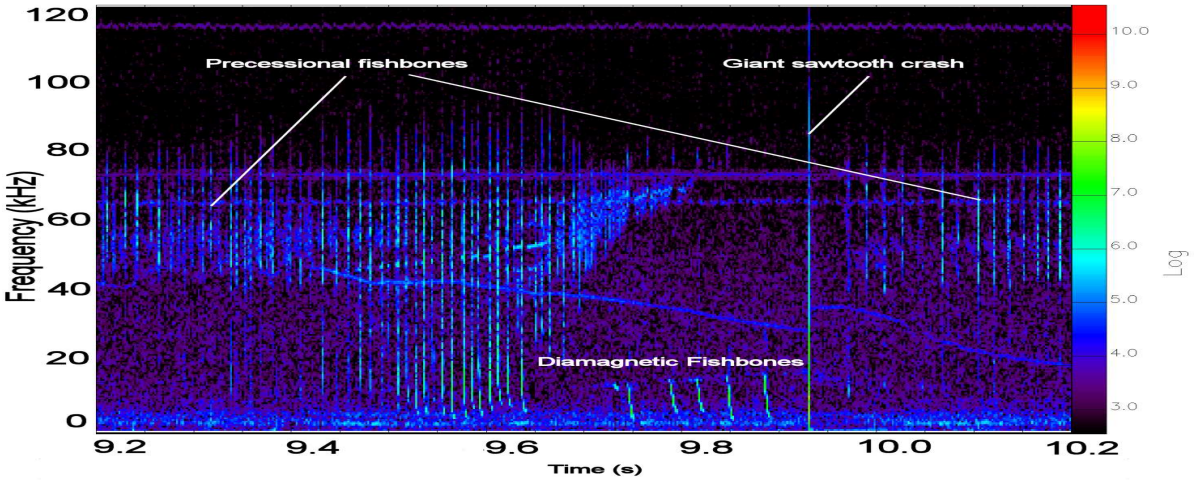

Figure 4: Spectrogram of MHD activity in pulse #54301

Sawteeth, diamagnetic and precessional fishbones are all caused by different branches of the solution of equation (5) and, in the ideal limit, the stability of these branches are governed mainly by the parameters $(\gamma_I, \omega_{*i}, \beta_h)$. Measuring or estimating the evolution of the parameters $(\gamma_I, \omega_{*i}, \beta_h)$ it is possible to explain the behaviour of these instabilities. In these discharges the regime where small sawteeth and precessional fishbones were observed must then correspond to the region of Fig. 2 where $\beta_h > \beta_{hc}$. In this region the kink branch as given by equation (5) should be stable, but this equation doesn't take account finite orbit width effects. These effects may allow the branch to be unstable. When the plasma density increases, the particles energy decrease reducing the size of the orbits. With this sawteeth may be stabilized but the fishbone branch remains unstable if $\beta_h > \beta_{hc}$. Stabilizing sawteeth stops the frequent crashes and both γ_I and ω_{*i} are allowed to increase. On one hand magnetic diffusion causes the radius of the q=1 surface to increase (γ_I scales with r_1^3 [23]) and on the other hand the absence of crashes allows the bulk ion profile to peak causing the diamagnetic frequency ω_{*i} to increase. The effect of an increase in ω_{*i} in the graphic of Fig. 2 is to move up the line $\gamma_I = \omega_{*i}/2$ and to reduce the maximum γ_M moving down the line $\gamma_I = \gamma_M$. With γ_I increasing and γ_M decreasing the condition $\gamma_I > \gamma_M$ will eventually be reached and when this happens the low frequency branch coalesces with the high frequency branch forming a single coalescent unstable branch. If $\gamma_I > \omega_{*i}/2$ the coalescent branch is the kink-fishbone, while if $\gamma_I < \omega_{*i}/2$ the coalescent branch is the ion-fishbone. The coalescent branches behave like the fishbone branch for high values of β_h and like the kink or ion branches for low values of β_h. To say it differently, increasing β_h pushes the coalescent branch towards the fishbone mode behaviour while increasing γ_I (ω_{*i}) pushes the mode toward the kink (ion) modes behaviour. Experimentally, after conditions $\gamma_I > \gamma_M$ and $\gamma_I < \omega_{*i}/2$ were reached, the coalescent mode still behaves as the precessional fishbone mode but this changes gradually as ω_{*i} increases. During each burst, β_h decreases temporarily inside the q=1 surface since fast ions are expelled from the plasma core. If β_h decreases enough, the mode behaviour may change from precessional to diamagnetic and a burst that started as precessional ends as diamagnetic. This mechanism is illustrated in Fig. 5. As consequence, hybrid fishbones with characteristics of both high and low frequency types that cover both ranges of frequencies are

observed (see Fig. 4 around t= 9.6 s). Every hybrid burst corresponds to a single event (see Fig. 6).

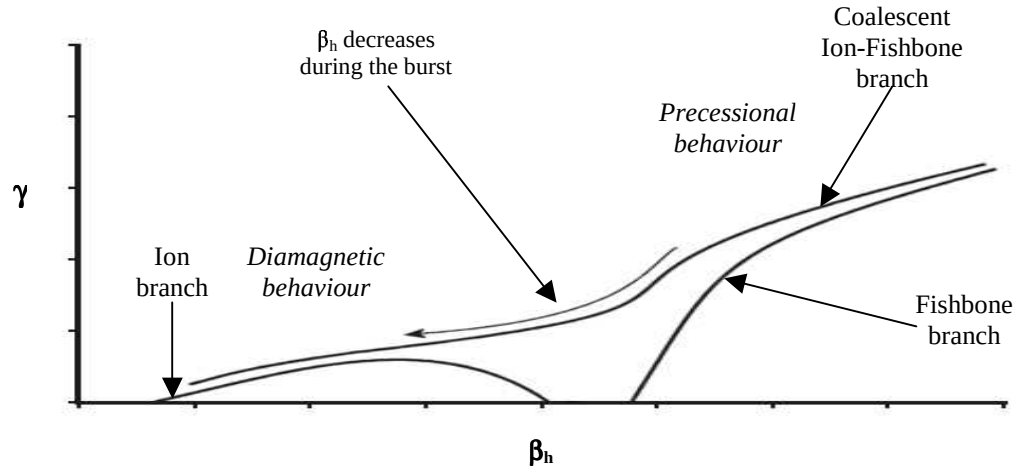

Figure 5: Schematic diagram of the solutions of the dispersion relation (5): Mode growth rate as function of the fast particles beta.

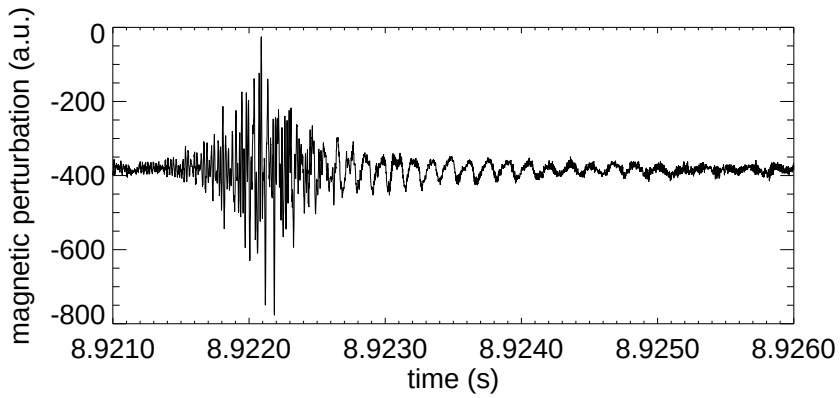

Figure 6: Temporal evolution of $\dot{\tilde{B}}$ for a single burst of hybrid fishbones (#54300).

Continuing to increase the diamagnetic frequency ω_{*i} brings the ion-fishbone branch to a regime where none of the behaviours dominates. When this happens both types of bursts can be triggered independently and they even occur simultaneously (see Fig. 4 around t= 9.75 s). Further increasing ω_{*i} the coalescent branch acquires the ion mode behaviour and only diamagnetic fishbones are observed. Diamagnetic fishbones activity ends when a monster sawtooth crash occurs. Since γ_I scales with r_1^3, a monster sawtooth crash would occur when the q=1 radius r_1 increases enough to verify $\gamma_I > \omega_{*i}/2$. The crash flattens the bulk ions' profile and reduces the q=1 size, restoring the original values of both γ_I and ω_{*i}. Precessional fishbones reappear and the whole cycle is repeated. Since the increase of the diamagnetic frequency is the base for the fishbone's cycle it is important to estimate its evolution along the cycle. The frequency in the laboratory frame $f_{*iLAB} = \omega_{*i}/2\pi + f_{rot}$ for the regime where frequent sawteeth crashes was estimated to be below 3 kHz. Since the diamagnetic bursts are initiated with a frequency around $\mathrm{Re}(\omega) \approx \omega_{*i}$ it is possible to observe that this value increases to around 10 kHz when diamagnetic fishbones are first observed and to near 20 kHz just before the monster sawtooth crash. This confirms that a steady increase of ω_{*i} occurs during the period of time between the crashes of monster sawteeth.

6. Summary and conclusions

A numerical code, using a perturbative approach, was employed to accurately calculate the hot particles functional δW_{HOT} as function of several parameters for a realistic geometry. In the limit $\omega/\langle\omega_D\rangle \to 0$ this allows the analysis of how sawtooth stabilization by fast ions depends on these parameters. Results show that the stabilizing effect associated with the non-adiabatic part of δW_{HOT} vanishes for small values of r_1 but not for larges values of r_1 while the destabilizing effect associated with the adiabatic part of δW_{HOT} increases with T_{HOT}. It was also shown that particles with potato orbits ($P_\phi < 0$) become important if the q=1 radius r_1 is very small. A variational approach was also used for a qualitative analysis. This method requires several simplifications but allows one to predict the stability of all branches, which depends mainly on ($\gamma_I, \omega_{*i}, \beta_h$). A new type of fishbones that covers both high and low range of frequencies was identified. These hybrid fishbones are caused by the coalescent ion-fishbone mode.

Aknowledgments
This work, supported by the European Communities and "Instituto Superior Técnico" under the Contract of Association between EURATOM and IST, has been carried out within the framework of the European Fusion Development Agreement. Financial support was also received from "Fundação para a Ciência e Tecnologia" in the frame of the Contract of Associated Laboratory. The views and opinions expressed herein do not necessarily reflect those of the European Commission, IST and FCT.

References

[1] – S. von Goeler, W. Stodiek and N. Sauthoff, Phys. Rev.Lett. **33**, 1201 (1974)
[2] – K. McGuire *et al*. Phys. Rev. Lett. **50** 891 (1983)
[3] – R. White, P. Rutherford and P. Colestock, Phys. Rev. Lett. **60**, 2038 (1988)
[4] – D. J. Campbell *et al*. Phys. Rev. Lett. 60, 2148 (1988)
[5] – M. Bussac *et al*. Phys. Rev. Lett. **35**, 1638 (1975)
[6] – G. Ara *et al*. Ann. Phys. (N.Y.) **112**, 443 (1978)
[7] – B. Coppi and F. Porcelli, Phys. Rev. Lett. **57**, 2272 (1986)
[8] – B. Coppi S. Migliuolo and F. Porcelli, Phys. Fluids **31**, 1630 (1988)
[9] – L. Chen, R. White and M. Rosenbluth, Phys. Rev. Lett. **52** 1122 (1984)
[10] – Y. Zhang, H. Berk and S. Mahajan, Nucl. Fusion **29**, 848 (1989)
[11] – D. Borba and W. Kerner, J. Computational Physics **153**, 101 (1999)
[12] – A. B. Mikhailovskii *et al*. Plasma Physics Reports **10**, 844 (1997)
[13] – W. Kerner *et al*. J. Computational Physics **142**, 271 (1998)
[14] – L. G. Huysmans *et al*. Phys. Fluids B **5**, 1545 (1993)
[15] – F. Porcelli *et al*. Phys. Plasmas, **1** (3), 470 (1994)
[16] – R. White *et al*. Phys. Fluids **26**, 2958 (1983)
[17] – R. White, L.Chen, F. Romanelli and R. Hay, Phys. Fluids **28**, 278 (1985)
[18] – R. White, M. Bussac and F. Romanelli, Phys. Rev. Lett. **62**, 539 (1989)
[19] – R. White, F. Romanelli and M. Bussac, Phys. Fluids B **2**, 745 (1990)
[20] – N. Gorolenkov *et al*. this conference
[21] – M. Mantsinen *et al*. Plasma Phys. Control. Fusion **42**, 1291, (2000)
[22] – T. H. Stix, Nuclear Fusion **15**, 737 (1975)
[23] – C. K. Phillips *et al*. Phys. Fluids B **4** (7), 2155 (1995)